Proceedings World Geothermal Congress 2020+1
Reykjavik, Iceland, April - October 2021

Geophysics over High Enthalpy Fields: Lessons from RLM-3D Magnetotelluric and Joint Inversions

Wolfgang Soyer[1], Randall L. Mackie[1], Stephen Hallinan[1], Federico Miorelli[1], Alice Pavesi[1], Stefano Garanzini[1]
Birean Sagala[2], Haris Siagian[2]

1) CGG Multi-Physics Imaging, Milan, Italy, 2) KS Orka Renewables, Jakarta, Indonesia

wolfgang.soyer@cgg.com, randall.mackie@cgg.com, stephen.hallinan@cgg.com, federico.miorelli@cgg.com, alice.pavesi@cgg.com, stefano.garanzini@cgg.com, birean.sagala@ksorka.com, haris.siagian@ksorka.com

Keywords: Magnetotellurics, static distortion, multi-physics, 3D inversion, cooperative inversion, joint inversion, Sorik Marapi

ABSTRACT

Practical data QC and 3D inversion workflows are now routinely available to reliably handle multiphysics datasets in quantitatively integrated 3D modeling. These result from direct project experience and related software development during hundreds of 3D projects with magnetotelluric (MT) and gravity data sets from many of the world's producing and prospective high enthalpy geothermal fields – as well as in other natural resource exploration markets. Our 3D inversion engine RLM-3D has evolved to address typical shortfalls and challenges of MT data sets, like separate locations for electric and magnetic sensors (sparse, telluric/T-MT surveys), or static distortions of electric fields: the code allows for accurate modeling of inter-station impedances, and joint inversions of galvanic distortion parameters along with the 3D resistivity. A number of regularization options allow tuning smoothing control to the specific exploration case; e.g. regularization tear surfaces to correctly account for sharp discontinuities at faults or other horizons.

RLM-3D also contains solvers for CSEM, gravity, gravity gradiometry, magnetics, and MEQ data (Vp, Vs, event re-locations), and therefore when available, these can be incorporated into the inversion modeling workflow, using a cross-gradient technique that promotes structural similarity between the inverted properties within a joint inversion. The same technology also provides for structural constraints from other sources, like geological, concept model scenarios under investigation, near surface dip and strike data to constrain shallow structural trends, fault surfaces, and seismic reflection volumes when available.

1. INTRODUCTION

Subsurface resistivity reflects primary lithology, secondary (hydrothermal) alteration grade and intensity, temperature, porosity and pore fluid salinity (Ussher et al., 2000; Cumming, 2009). Broadband Magnetotellurics (MT) surveys today, responding to the 3D resistivity distribution from surface down to tens of kilometers depth, are therefore the most commonly employed geophysical technique during geothermal resource exploration. The applied geophysics also include ground gravity and magnetics, mapping density and magnetic susceptibility, Time Domain Electromagnetics (TDEM), Controlled Source Audiomagnetotellurics (CSAMT), Vertical Electrical Soundings (VES, DC) mapping shallower resistivity with respect to MT, and heliborne gravity gradiometry (HAGG), TDEM and magnetics (e.g. Feijth et al, 2018) and airborne tipper (ZTEM, compared to MT in Soyer et al 2018).

During production and development phases, repeat precision gravity / levelling surveys and continuously recording microearthquake arrays (MEQ) are increasingly deployed, monitoring fluid saturation changes, production v. recharge balances and microseismic event patterns and characteristics reflecting rock/fluid interactions and pressure/stress changes.

Following on from recent work on the MT, gravity and MEQ data from the Darajat field (Soyer et al 2017, 2018a) we further illustrate here the pros and cons around quantitative integration of different geophysical datasets through joint inversion modeling. As MT data is often the dominant (or only) type available we first discuss practices in analyzing MT data both in terms of data preparation and inversion modeling, before addressing the multiphysics domain.

While structural correlations between different physical property distributions (e.g. resistivity, density, velocity) are expected in straightforward geological settings, the petrophysical relationships vary across the geological spectrum (e.g. tight lava and dry pumice are both resistive, but have very different density and velocity relationships). The cross-property links in joint inversion schemes should allow, for example, opposite polarity of changes across property boundaries, or absence of a change in one parameter where another one is changing. The cross-gradient method introduced by Gallardo and Meju (2003) addresses structural similarity over hard petrophysical links, and has been implemented in our RLM-3D inversion modeling suite as one of several inversion regularization constraints.

In addition to a flexible global model smoothing constraint, more granular options can also be used, such as adding additional near-surface smoothing or specifying directional factors on regularization for whole or specific regions of the model. Especially important for potential field methods is the ability to add extra depth-dependent regularization similar to Li and Oldenburg (1998) which is used to suppress the tendency of an inversion to put all model detail at shallow depths and encourage deeper model changes (gravity data can be fit with a thin sheet of density variations at the surface). Model bounds can be specified for any domain but we have found that using variable bounds (different bounds for different parts of the model) are especially valuable for gravity inversions. A more explicit way to provide a priori information is by damping changes for certain model parts that are included in the start or a priori model. This is controlled with a trade-off parameter that sets the damping to be higher (in other words, fixing the model values at their start or a priori values) or lower, which allows some variation away from the set values.

The smoothness regularization of the 3D inversion can optionally be interrupted across so-called tear-surfaces: while to either side of such surfaces smoothing regularization is applied, a sharp change is allowed across the surfaces. The tear concept is implemented in a way that it allows finite, open surfaces to be used as a basis for their definition – at the edge of the surface, also the tear ends.

2. ASPECTS OF MAGNETOTELLURIC DATA ANALSYSIS

2.1 Layout considerations

The electric field measurements (the "telluric" in MT) require grounded dipoles typically around 100m length to get high enough signal levels. While the dipoles are often extended across steep terrain and/or laterally variable near-surface resistivity, the finite length is treated as a point source by most modeling codes, and despite earlier investigations (e.g. Pellerin and Hohmann, 1990; Poll et al, 1989) the topic has received little attention recently. We have recently looked at the effect of the dipole extent on measured data in several 3D model scenarios, including steep topography and strongly variable near-surface structure (Soyer et al., 2018c, 2019). The electric fields were integrated along the dipole lines in finely discretized models and divided by their length, and the resulting field estimates compared with solutions at the central surface cells of the dipoles. Effects are significant when the two electrodes are in different geo-electric environments – mainly 1) steep topography, and 2) outcropping structure, and therefore different resistivity at each dipole electrode. Topography causes distortions that have a significant inductive (phase) component at frequencies down to 0.01Hz. Dipole effects from outcrops or faults may be stronger, especially when associated with current channeling, but are also essentially subsumed in the distortion model at low frequency (Soyer at al., 2019). For strong variation underneath a continuous cover – for example sharp thickness variations of a conductive over – the effects are weaker.

An aspect of the measurement typically ignored is that it is done along the topographic slope, whereas modeling codes use the horizontal field component. This would require an amplitude correction of the inferred impedances, in order to scale down to the horizontal component.

In summary, the differences between finite dipole solutions and modelled point solutions can largely – at frequencies <0.01-0.1Hz – be described by the galvanic distortion model for electric fields, as already pointed out by Pellerin and Hohmann (1990), and for 3D MT inversions, the more convenient approach of using local solutions for electric fields, as done also in RLM-3D, is well justified.

In some surveys, not all channels of the data transfer functions are co-located, and magnetic channels are from a different location – either by survey design e.g. for safety reasons, or due to sensor failures at certain MT setups. In these T-MT (telluric-magnetotelluric) like situations, the true positioning of all channels is taken into account, and transfer functions calculated in the inversion process are indeed computed from electric and magnetic fields at different locations.

2.2 Galvanic Distortion and Topography

An inherent quality of magnetotelluric data is that electric field data may be subject to frequency-independent amplitude distortions, known as galvanic distortions. These originate from small-scale structure that will not be successfully resolved in a 3D inversion, and are also in the context of the measurement layout, as discussed above.

Often with the original intention to provide a means to correct MT data for static distortions affecting electric field measurements (Pellerin and Hohmann, 1990), co-located central loop time domain (TDEM) may be available over a geothermal field, in particular for legacy data sets. These corrections can be essential for 1D layered earth inversions.

However, in a 3D context, it also constitutes a tampering with observed data to address a phenomenon that is inherent in the MT method. Furthermore, TDEM data themselves are subject to effects from structural inhomogeneities and topography, and inversions of these data may lead to unrepresentative one-dimensional models (Watts et al., 2013). In 3D inversions, the requirement to account for galvanic effects in data input is more questionable, as the inversion can account for this remarkably well via inclusion of small-scale structure, while smoothing contains the impact on deeper structure (Soyer et al., 2008, and synthetic example presented here). In fact, 3D inversion results from TDEM-corrected MT data using the above method typically compare well with those using original data. For contrasts of a somewhat larger scale, including topographic effects, it becomes rather more accurate to feed the original impedance tensors to the inversion.

For MT data with severe distortion effects, RLM-3D allows for a direct inversion for static distortion parameters (Soyer et al., 2018b). The galvanic distortion is represented by site-specific real-valued 2x2 matrices acting on the electric fields and therefore impedances across the entire frequency band, and the distorted tensor Z_C can therefore be written as:

$$Z_C(f) = CZ(f) = \begin{pmatrix} C_{11} & C_{12} \\ C_{21} & C_{22} \end{pmatrix} \begin{pmatrix} Z_{xx}(f) & Z_{xy}(f) \\ Z_{yx}(f) & Z_{yy}(f) \end{pmatrix} \quad (1)$$

where Z is the 2x2 complex impedance tensor between the undistorted horizontal electric field and the magnetic field in frequency (f) domain, and C is the real-valued, frequency independent 2x2 distortion matrix.

Inversion is simultaneous for 3D resistivity structure and distortion matrices, with a control parameter that suppresses deviations from the identity matrix, which represents the a priori condition of no distortion. With a very high value, distortions are suppressed and only significant when very strongly required by the data; with a very low value instead, the inversion is freer to introduce impedance rotations and shifts in order to fit the data, rather than via resistivity structure. The distortion matrix estimation is therefore intrinsically linked with the structural smoothing constraint of the 3D inversion, and an intermediate choice will find the right balance between structure and distortion parameter estimations.

2.3. Inversion Preparations

Meticulous data revision is a key step prior to inversions, removing data segments judged unreliable. Input data to 3D MT inversions are full tensor complex impedances and magnetic transfer functions. If of poor quality, re-processing of the original time series to the MT transfer functions, using remote reference, robust, signal-noise separation methods can improve the data input pre-inversion. Common noise sources include active or passive noise from ground installations, layout errors, capacitive effects due to high electrode contact resistances, etc.

Minimum-structure 3D inversions like RLM-3D require smoothness constraints to control model structure, and the parameter choice for these constraints determines the inversion outcome to a good extent. Comparisons with 1D inversions for shallow structure serve as a guide in choosing vertical model discretization and regularization, while the objective is explicitly not to reproduce the false 1D layering. A balance is required to arrive at reliable models that contain the detail necessary to reproduce data observations to the desired extent, while suppressing artefacts. Practically, this entails performing a suite of 3D inversions, where subsequent runs start from the previous outcome but use successively lower regularization constraints.

Tietze and Ritter (2013) demonstrated a dependency of 3D inversion results on the orientation of input data tensors, in a regionally two-dimensional setting, and with favorable results for deeper, dyke-like structures when the data orientation is aligned with these. Although we have seen little variation of 3D inversion results with changes in data orientations over several areas, we generally aim at rotating data to the prevailing regional strike direction, if a clear regional 2D context is present. Another aspect to take into account however is also the setup orientation; data are most typically acquired using a geo-magnetically aligned layout. When left unrotated, errors for the impedance transfer function estimates relate more closely to the single channels involved, and editing of individual tensor components in the data preparation for inversion can address channel failures in a direct way (e.g. a noisy electrode resulting in poor measurements along one dipole only). With this in mind, we perform a survey-by-survey judgment on whether to model MT data in the original orientation or using a data orientation aligned with the prevailing regional structure. Similarly, the rectilinear 3D inversion mesh is preferably oriented to the main geo-electric strike direction, if present, but if the site distribution results in much reduced total mesh, then the mesh orientation will be adjusted accordingly. Technically, in RLM-3D, there is no requirement to orient input data tensors to the mesh direction: RLM-3D rotates calculated responses to the orientation of the input data before estimating sensitivities.

3. INTEGRATED 3D INVERSIONS

Integrated inversion may be either cooperative or joint (simultaneous). In a cooperative joint inversion, the result from one data type's inversion is integrated as a priori information into the inversion of the other type. In RLM-3D, this may be accomplished by using structural cross-gradient constraining to a previous inversion result, which will promote structural similarity in the inversion of data type 2 with inversion results from data type 1. In a joint inversion, data and model vectors of the inversion are the combination the single type ones, and the inversion will update both properties at each iterations of the process. When further structural information is available, this can also be used to constrain a joint inversion. In this case, the two geophysical properties are linked via cross-gradients, and each or one of these is additionally linked to the reference model.

Labelling the data misfit and model regularization terms Φ^{data} and Φ^{reg}, and cross-gradient terms between the model properties Φ^{xg}, the objective function for a joint inversion takes the general form:

$$\Psi(\vec{\mathbf{m}}) = \sum_{j=1,2} \alpha_j \Phi_j^{data} + \sum_{i=a,b} \lambda_i \Phi_i^{reg} + \tau_{a,b}\, \Phi_{a,b}^{xg} \quad \left[+ \sum_{i=a,b} \tau_{i,ref} \Phi_{i,ref}^{xg} \right] \tag{2}$$

where $\vec{\mathbf{m}}$ is an ensemble of model properties (a, b). Indices j refer to different data types. Factors α, λ, and τ weight the contribution of the respective terms to the objective function (Commer and Newman, 2009). For the data weights, the ratio between the total numbers of data points of the two methods involved is used, but the weight can be adjusted.

While here we present the cross-gradients as a way of integrating the different data types, both in a cooperative and in a joint workflow, there are several other ways to integrate diverse data types. Velocity and density models are often converted using empirical relationships (e.g. Gardner, Nafe-Drake), tuned from well logs using cross-log analysis; suitable logs, however, are rarely available at geothermal fields. Alternatively, a gravity model may be updated by importing structure obtained from MT inversions, and then subsequently inverted.

4. EXAMPLE CASES

In order to demonstrate some of the data inversion aspects outlined above re MT and inversion regularization, firstly a generic, stand-alone synthetic study is examined, followed by a joint analysis of measured MT and gravity data from the Sorik Marapi geothermal field, located in Sumatra and operated by KS Orka Renewables.

4.1 Simulation of a Geothermal Field with graben

Using real topography (only) borrowed from a similar setting, a conceptual geothermal field was built over a caldera region located northward of an extinct volcano, with an up-doming of a resistive and dense reservoir zone over a conductive and lower density clay cap. Similar to settings along the Sumatra fault, the simulated field is adjacent to a major graben structure (Figure 1). A typical three-layer scenario was configured to the east of the graben, and its west is characterized by resistive and denser rock without alteration signature. Rock properties in the graben have a similar layering as in the east, but with slightly different values and different depth levels.

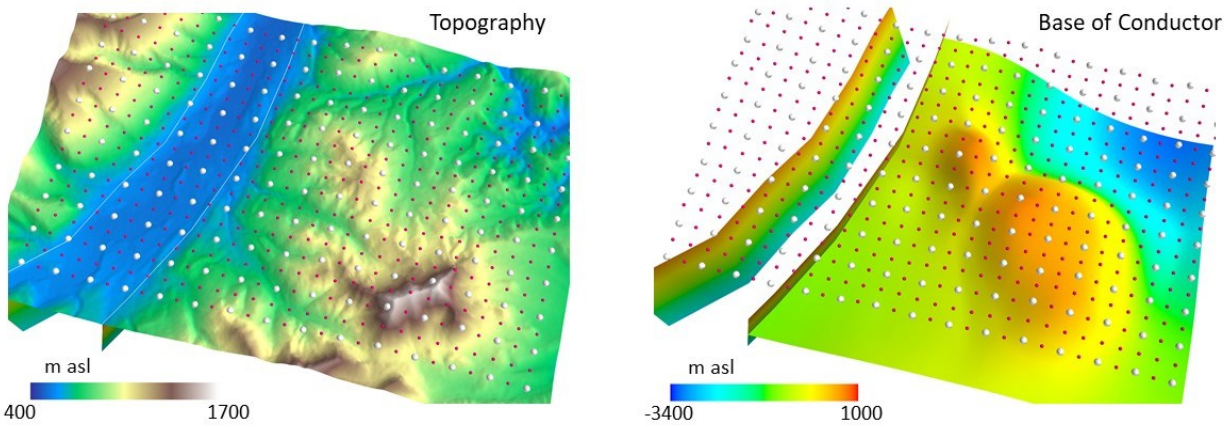

Figure 1. Structural setup for the synthetic study. Left: topography with fault outcrops and MT (white) and gravity (red) stations. Right: graben faults, and base of conductor topography under the simulated geothermal field.

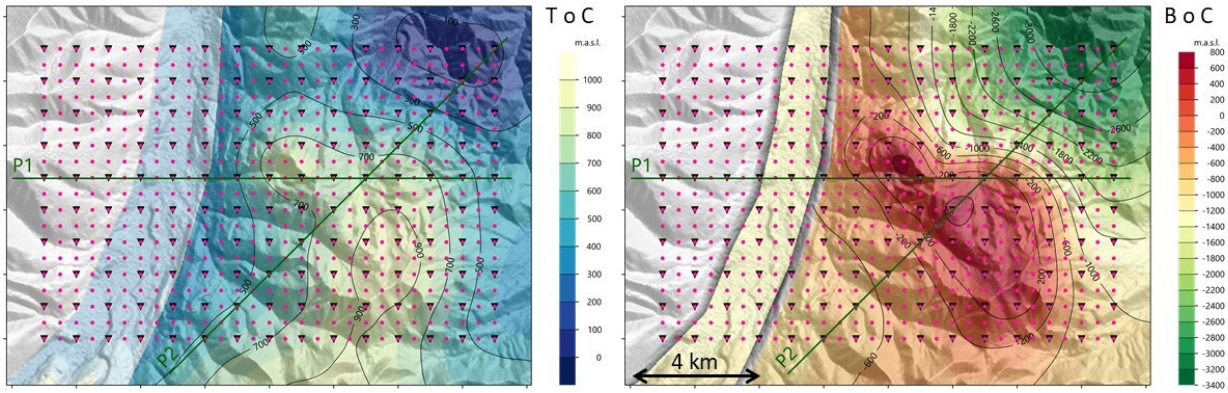

Figure 2. Map view of the conductor surfaces: top (left) and bottom (right). Also shown are site locations (triangles=MT, circles=gravity), and profile locations.

The total topographic range covered is about 1100m. The smooth top surface of the clay cap is placed at 50-750m below ground level, and its thickness varies considerably from 120m to 3400m, due to the strong topography of its base (Figure 2). Within the graben, the zone with alteration and/or sedimentary signature extends from 300m to 1500m bgl. Rock properties are summarized in the table below, and initial properties – note the gradient for density – in inversions are listed at the bottom.

	resistivity	**density**
east – shallow	50-300 Ωm [lateral variation]	2.40 g/cc
east - clay alteration zone	1-3 Ωm [lateral variation]	2.20-2.30 g/cc [lateral variation]
east - below cap (reservoir)	250 Ωm	gradient: [2.50, 2.67] g/cc in 4km
graben – shallow	50 Ωm	2.10 g/cc
graben – intermediate	2 Ωm	2.20 g/cc
graben – deep	as to the east	as to the east
west	500 Ωm	gradient: [2.50, 2.67] g/cc, 4km
< -10,000m asl	10 Ωm	(2.67 c/gg)
initial properties	20 Ωm	gradient: [2.40, 2.67] g/cc, 5km

Property variation is mostly congruent between resistivity and density, except for the shallow graben fill, where a low density was set (2.10 g/cc), at moderate resistivity (50 Ωm). Properties were smoothed within the graben and independently to the east, but the contrast across the faults is sharp. A constant density of 2.40 g/cc was subtracted from the density model, in order to simulate Bouguer responses and reduce topographic discretization effects.

MT sites were spaced 1km apart, and gravity measurements were sampled at 500m. Forward modeling was performed using a 100m x 100m mesh, with 25-100m layering vertically (topography / deeper zone of interest). The MT frequency range covers 0.001-1000Hz, with a density of 5 frequencies per decade, and the same frequency set was used in inversions. A Gaussian error of 4% and 0.02 standard deviation was given to MT impedances and magnetic transfer functions (“tipper”) and an error of 0.2 mGal to the calculated gravity response.

The graben faults on either side can be explicitly included in the inversion process by applying a tear (discontinuity) in the smoothing function (regularization) across the fault surfaces, which for the inversion extend down to 3km depth. This allows for sharp resistivity changes across the fault, while structure is required to be smooth away from the fault on either side, as usual. Below, the smoothing constraint is again omnidirectional.

4.1.1 Inversion of Distorted MT Data

The calculated MT data were further subject to strong distortion, using the parameter decomposition concept of Groom and Bailey (1990), and the same limits for uniformly distributed random numbers used by Soyer et al. (2018b) of ±0.5, and ±45° and ±30°, for anisotropy, and twist and shear angles, respectively. A logarithmically uniform distributed gain error was further applied, within bounds of half an order of magnitude.

MT single domain inversion results between undistorted and distorted data are summarized in Figure 3 along SW-NE line P2. Undistorted data are inverted to an accurate resistivity model – compare with contours shown on the 1D plot – and good data fit. To illustrate the strength of the distortion applied to the data set, 1D inversions of the tensor invariant determinant are overlain on the section as colored sticks, using the same resistivity color scale. These would indicate a wildly differing resistivity layering, and without 3D inversion, interpretation of these data would be very challenging. 3D inversion of the data in contrast provides fairly reliable results although data are fit only to an rms of ~2.8, and the main impact is a high shallow lateral resistivity variation. When inverting additionally for static distortion parameters, the shallow variability is attenuated, the deeper structure is more accurately modeled and the data fit improves considerably.

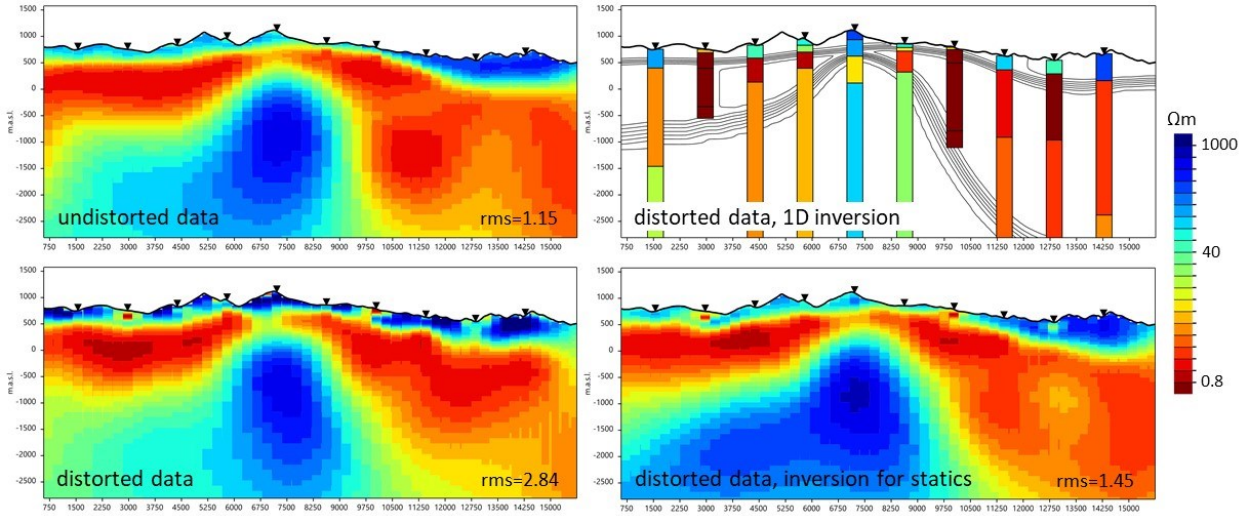

Figure 3. Synthetic example, profile P2. The effect of galvanic distortions on 1D and 3D MT inversion results (see text for discussion). VE=1.5.

4.1.2 Single Domain Inversions

Figure 4 shows initial properties along W-E line P1 that crosses the graben, as well as unconstrained inversions (i.e. starting with a uniform half space fill) with and without the use of regularization tears at the faults. Undistorted data with errors were used as input. While some detail of the conductor base is missing, the resistivity structure poses no major challenge to MT inversion, and the true model is fairly well recovered. For gravity, the lateral variation in lower density reflects the true setting well, but without further constraining, the results lack depth control. Because the starting density has overall higher values than the true model, modelled densities are too high on average, which is true for all gravity models presented here. Use of regularization tears at the main faults results in sharp changes to the graben flanks – primarily to the west, and for gravity, which has a stronger integrated density change across the fault, also to the east. Structure recovery certainly improved with the use of the tears.

4.1.3 Cooperative and Joint Inversions

Both cooperative and joint 3D joint inversions were performed. All these inversions made use of regularization tears for the fault down to 3km (Figure 5). For the cooperative inversion, the MT single domain inversion result shown above was used as a structural reference in a subsequent gravity inversion. In the central model area, the recovered density structure has improved significantly over the single domain gravity inversion. Contours show the structural similarity with the reference MT model (top left). In the graben, the low-density zone is modelled as a focused anomaly like the MT, and – as in all the gravity inversions presented – the surface very low density layer, anti-correlated with resistivity, cannot be resolved.

It is worth mentioning that this integrated gravity modeling is computationally very fast to perform, since it involves only gravity calculations at a fairly small number of data points over a medium sized 3D grid. Joint inversions are mathematically more complex, and balancing convergence of both data types, over significantly more iterations, can be challenging to achieve. Results may be superior to cooperative inversions, however, especially if these involve only a single step as done here (Figure 5). Structure in the joint inversion aligns more consistently that in the cooperative approach.

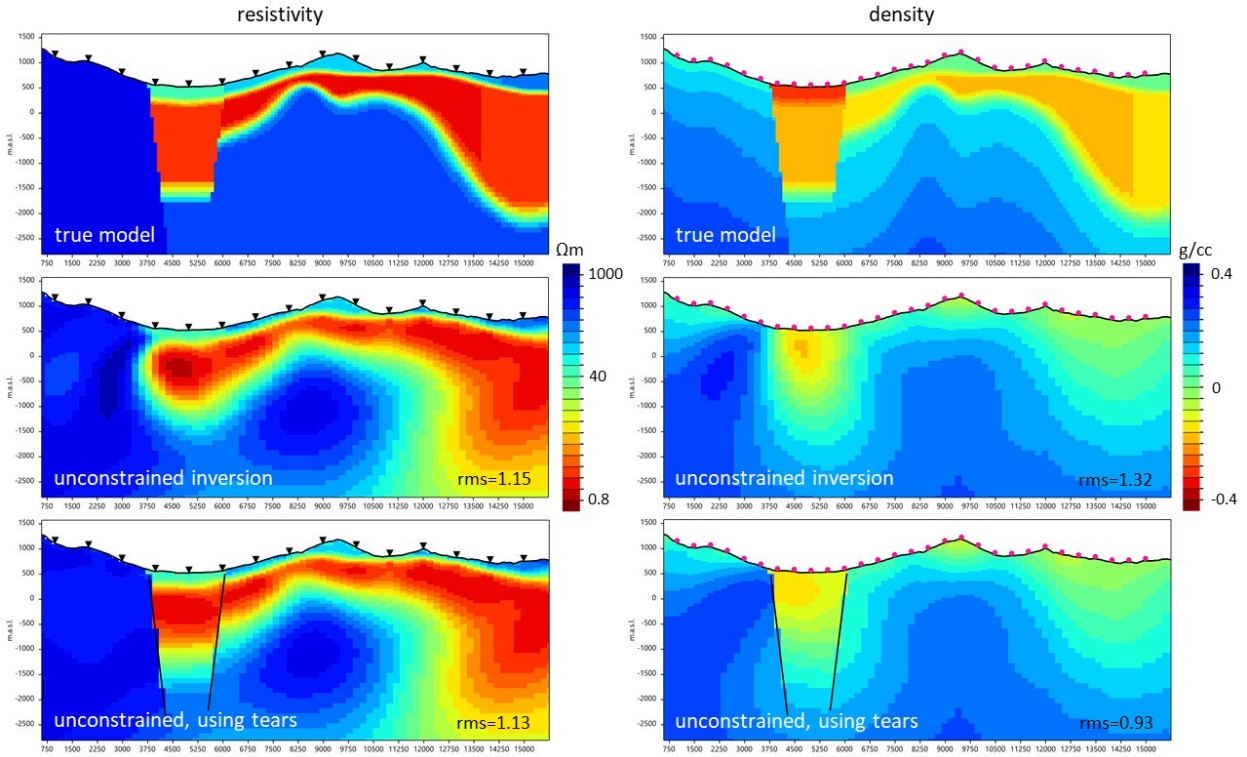

Figure 4. Synthetic example, profile P1. Unconstrained single domain inversion results of MT (left) and gravity data (right). The top row shows the true model structure, used to calculate the synthetic data set, which was then given Gaussian errors prior to inversions. Below, inversion results are presented without (center) and with (bottom) use of the faults as tear surfaces for the structural regularization. Density values are with respect to the reference value of 2.4 g/cc. Vertical exaggeration (VE) is 1.5.

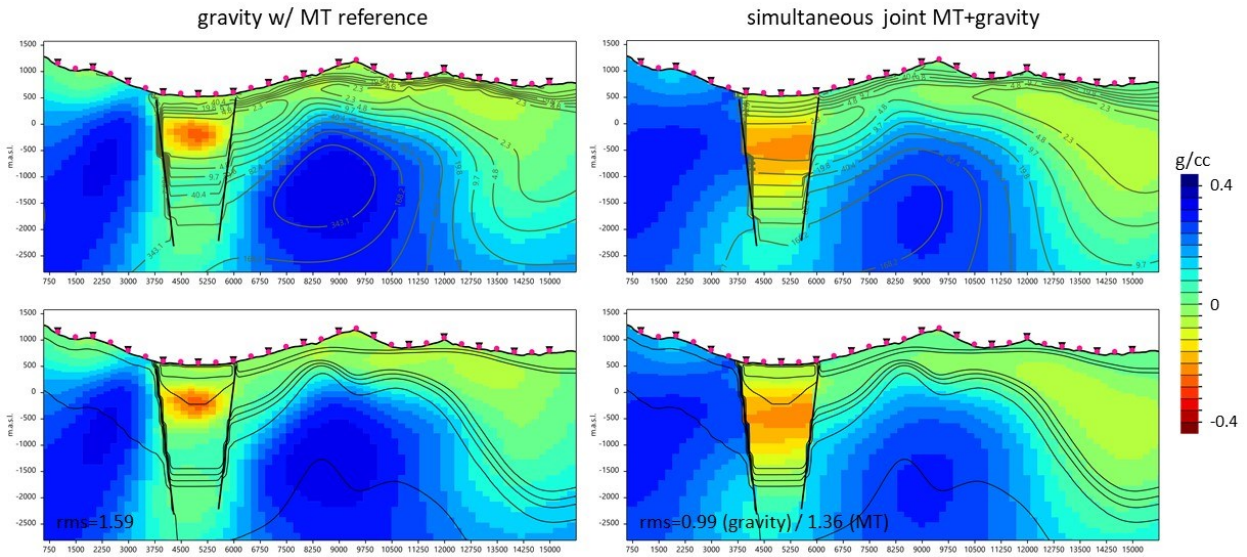

Figure 5. Synthetic example, profile P1. Inversion results along profile P1 involving cross-gradients with MT. Left: Gravity inversion, using cross-gradient constraining to the MT single domain 3D inversion result, as a reference. Right: Density from joint gravity+MT 3D inversion. Top shows contours from corresponding resistivity model; at the bottom row, true density model contours are shown. All inversions used a regularization tear at the fault locations, down to 3km depth. VE=1.5.

4.2 Real Data Case: Sorik Marapi

The Sorik Marapi geothermal field is located in the southeast of the Panyabungan pull-apart basin, but unlike the synthetic case illustrated before, here the geothermal field is located *within* the graben structure. The basin is compartmentalized into different, deep graben units, filled with a thick pile of volcanic sedimentary material from the onset of volcanism until present day volcanic activity from the nearby Sorik Marapi volcano (Sagala et al., 2016, Rezky and Hermawan, 2015). Rocks to either side of the graben are pre-Tertiary metamorphic units. The field is in the development phase, with a planned full target capacity of 240 MW.

In 2018-2019, subsequent to new data acquisition of both MT and gravity data, CGG performed integrated 3D inversion modeling of the new data, adding in the MT and gravity data from earlier field surveys. All inversions were carried out using RLM-3D, and both single domain and joint inversions were performed.

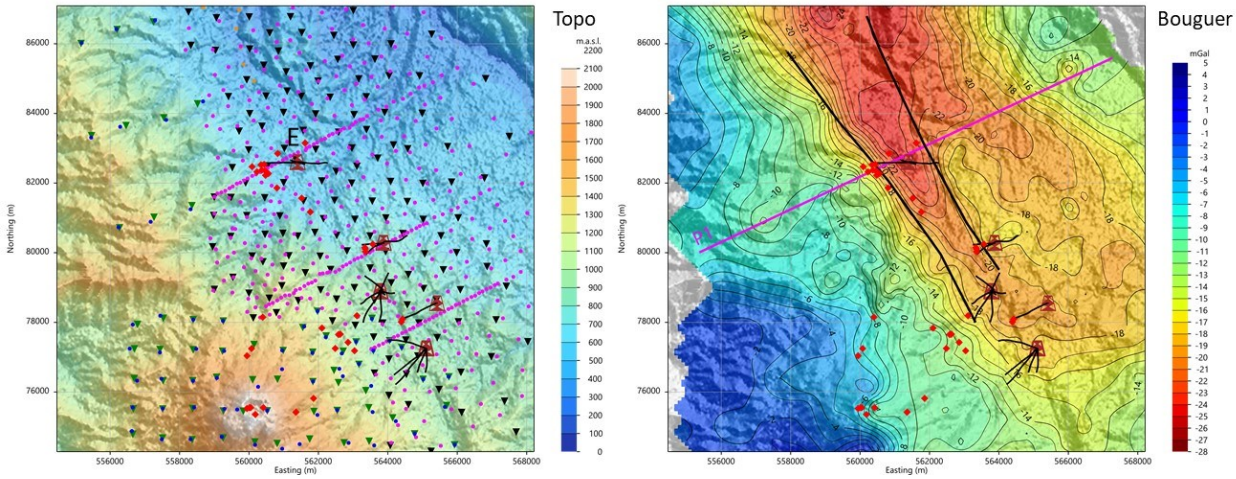

Figure 6. Sorik Marapi geothermal field, Sumatra. Map shows combined data sets of MT (triangles) and gravity (points) data from several geophysical surveys to the north and east of the Sorik Marapi volcano (located on the southern margin of the maps). Right: Complete Bouguer gravity anomaly at reduction density 2.40g/cc (note reverse color scale). Also shown are well pads (brown) with well traces (black), of which the one on line P1 (pink) is pad "E". The two black NW-SE lines mark faults, picked from structural mapping as well as tracing gravity gradient maxima.

The Bouguer gravity map provides information on the deepening of the graben in certain areas, as well as the graben lateral boundaries, where the strongest gradients are observed (Figure 6). We have inferred fault traces from structural maps and locations of gravity gradient maxima, and generated normal fault surfaces with an ad hoc, steep dip of 80 degrees. With a depth extent of 3km, these were used to build finite length regularization tears, deployed in a subset of the inversion runs. Bouguer gravity data were inverted, assigning a 0.3mGal error, modeling relative density changes with respect to the reduction density. MT data were modeled within the frequency band of 0.0016-2500Hz, with five frequencies per decade.

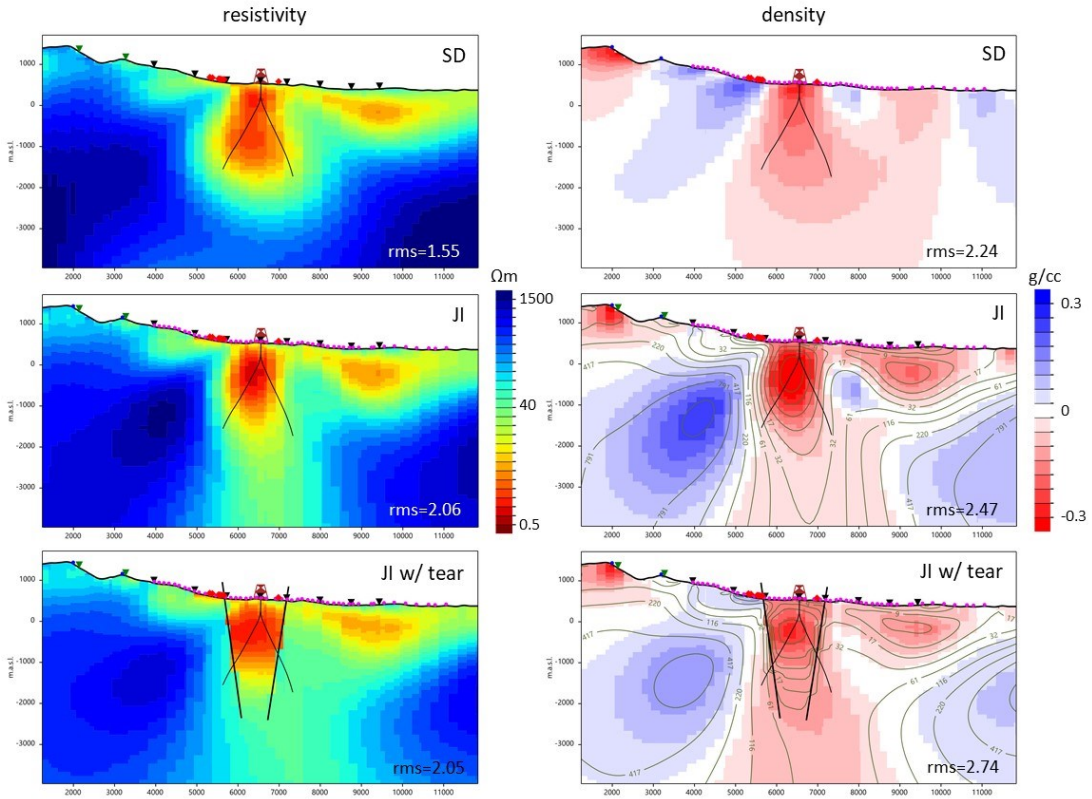

Figure 7. Sorik Marapi, 3D inversion results along line P1 with well "E". Top: single domain MT (left) and gravity inversion (right). Center and bottom rows show joint MT+gravity inversion results of both data sets, with cross-gradient constraining between the two properties. Results shown at the bottom involve regularization tears at the inferred fault location, extended 3km down, at a dip of 80 degrees. Density values are relative with respect to a reduction reference density of 2.4 g/cc. No vertical exaggeration.

Results from these inversions are shown along the SSW-NNE line P1 shown on the map, which passes through wellpad "E" (Figure 7). No other information was used as a priori constraints. As in the synthetic example and typical for this combination of data types, the MT result is comparably more robust, with little difference between single domain and joint, except at greater depths, while gravity inversions improved considerably with the inclusion of shallow depth information from the MT models, producing improved imaging of the low density basin fill. The use of fault surfaces as regularization tears results in a sharp boundary specifically at the western limit of the graben, and accordingly less artifacts (lower overshoot to higher resistivity) from the smoothing. Traces of the two wells at pad "E" should intersect with this graben boundary definition, however from the analysis of cuttings there has been no clear rock contrast identified that would be interpreted as a fault. One set of methylene blue (MeB) data from the eastern well "E" became available after the inversion runs; the results plotted here in Figure 8, overlain on the joint inversion with tears, show excellent correlation with the resistivity break at the presumed fault location.

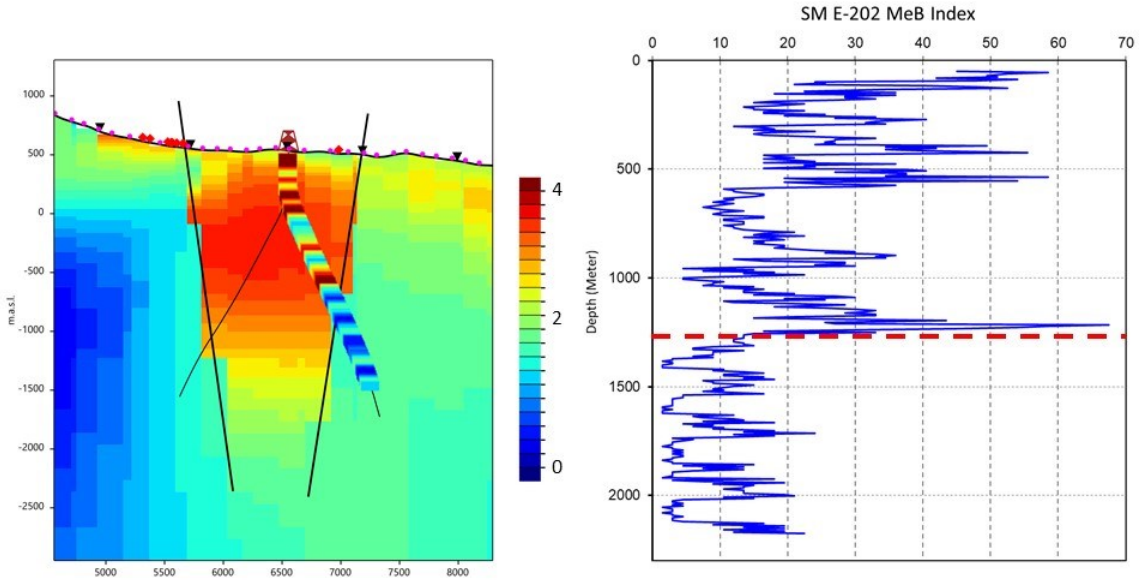

Figure 8. Sorik Marapi profile P1, showing the good correlation between the 3D MT inversion resistivity and well cutting methylene blue contrasts across the proposed fault location. The resistivity color scale is as in previous figure, and the colorbar refers to the smoothed MeB readings along the well.

5. CONCLUSIONS

Through integrated modeling of multiple geophysical data types over geothermal fields, we ultimately aim at deriving a geologically reliable multi-property 3D model that consistently explains the observations of each geophysical dataset. Since analytic, petrophysical relations between density and resistivity are far from straightforward in geothermal settings, varying across different lithology types, we impose a structural similarity constraint between them using a 3D cross-gradient implementation. Inclusion of a priori information, if available – like density logs from wells, or a porosity volume from a geophysical concept model – allows further constraints on the 3D inversion. The latter approach can also be used to test different scenarios or concept models, finding those that are consistently in agreement with the observed data available.

We presented both cooperative and joint inversion examples for MT and gravity data, firstly for a synthetic, and then a real data scenario. While MT results were largely similar for both single and joint domain inversions, gravity inversions – with inherently weaker depth sensitivity than MT – benefited significantly from the integration, in both cooperative and joint workflows. In the synthetic example, the joint approach yielded preferable results, albeit with much greater numerical effort than when using the MT result cooperatively. Further improvements are expected with the use of appropriately set density bounds, and the building of more detailed starting or a priori models that bring the starting point for the inversions closer to the actual setting, and result in more accurate absolute density estimates.

For MT data inversions in their own right, we have built solid 3D data analysis and inversion workflows, with robust means to deal with rugged topography and galvanic distortion effects, yielding increasingly reliable complete earth resistivity volumes.

ACKNOWLEDGMENTS

The authors would like to express their gratitude to KS Orka Renewables for the permission to publish the results from the 3D inversion modeling of the Sorik Merapi geophysics data.

REFERENCES

Commer, M., and Newman, G.A.: Three-dimensional Controlled-Source Electromagnetic and Magnetotelluric Joint Inversion, *Geophysical Journal International*, **178**, (2009), 1305-1316.

Cumming, W.: Geothermal Resource Conceptual Models Using Surface Exploration Data, Proceedings, *34th Workshop on Geothermal Reservoir Engineering*, Stanford University, Stanford, CA (2009).

Feijth, J., Hope, J., Ninomiya, A., Ishikawa, H., Shirota, A., Takuji, M., and Nakamoto, G.: Interpretation of Heliborne AGG, EM and Magnetic Data for Geothermal Exploration in the Musadake-Teshikaga Area, Proceedings, *13th SEGJ International Symposium*, Tokyo, Japan (2018).

Gallardo, L.A., and Meju, M.A.: Characterization of Heterogeneous Near-Surface Materials by Joint 2D Inversion of DC Resistivity and Seismic Data, *Geophysical Research Letters*, **30**(13), (2003), 1658.

Groom, R.W., and Bailey, R.C.: Decomposition of Magnetotelluric Impedance Tensors in the Presence of Local three dimensional Galvanic Distortion, *Journal of Geophysical Research*, **94**, (1989), 913–1925.

Jiracek, G.R.: Near-surface and Topographic Distortions in Electromagnetic Induction, *Surveys in Geophysics*, **11**(2-3), (1990), 163-203.

Jones, A.G.: Static Shift of Magnetotelluric Data and its Removal in a Sedimentary Basin Environment, *Geophysics*, **53**(7), (1988), 967-978.

Mackie, R., and Watts, M.D.: Detectability of 3-D Sulphide Targets with AFMAG, *Extended Abstract*, SEG Annual Meeting, Las Vegas, NV (2012).

Mackie, R.L., Miorelli, F., and Meju, M.A.: Practical Methods for Model Uncertainty Quantification in Electromagnetic Inverse Problems, *Extended Abstract*, SEG Annual Meeting, Anaheim, CA (2018).

Meju, M.A., Mackie, R.L., Miorelli, F., and Shahir Saleh, A.: Crossgradient Anisotropic 3D CSEM Inversion Integrated with Seismic and Well Log Data to Reduce Uncertainty, *Extended Abstract*, SEG Annual Meetings, Anaheim, CA (2018).

Li, Y., and Oldenburg, D.W.: 3-D Inversion of Gravity Data, *Geophysics*, **63**(1), (1998), 109-119.

Lin C., Zhong S., Auken E., Cai H., Tan H., Peng M., Kong W.: The Effects of 3D Topography on Controlled-Source Audio-Frequency Magnetotelluric Responses Two-Dimensional Topographic Responses in Magnetotellurics Modeled Using Finite Elements, *Geophysics*, **83**(2), (2018), WB97-WB108.

Patzer, C., Tietze, K. and Ritter, O.: 3D Modelling and Inversion using Elongated Electric Field Receivers, *Extended Abstract*, 24th EM Induction Workshop, Helsingør, Denmark (2018).

Pellerin, L., and Hohmann, G.W.: Transient Electromagnetic Inversion: A Remedy for Magnetotelluric Static Shifts, *Geophysics*, **55**(9), (1990), 1242-1250.

Rezky, Y., and Hermawan, D.: Geothermal System of Sorik Marapi - Roburan - Sampuraga, North Sumatera, Indonesia, Proceedings, *World Geothermal Congress*, Melbourne, Australia (2015).

Sagala, B.D., Chandra, V.R., and Purba, D.P.: Conceptual Model of Sorik Marapi Geothermal System based on 3-G Data Interpretation*, ITB International Geothermal Workshop*, Bandung, Indonesia (2016).

Scholl, C., and Miorelli, F.: Otze – Airborne EM Inversion on Unstructured Model Grids, *AEM, 7th International Workshop on Airborne Electromagnetics*, Kolding, Denmark (2018).

Soyer, W., Hallinan, S., Mackie, R.L., and Cumming, W.: Statics in Magnetotellurics – Shift or Model? *70th EAGE Conference and Exhibition*, Rome, Italy (2008).

Soyer, W., Mackie, R.L., Hallinan, S., Pavesi, A., Nordquist, G., Suminar, A., Intani, R., and Nelson, C.: Multi-Physics Imaging of the Darajat Field, *Geothermal Research Council Annual Meeting*, Salt Lake City, UT, *Transactions*, 41, (2017).

Soyer, W., Mackie, R.L., Hallinan, S., Pavesi, A., Nordquist, G., Suminar, A., Intani, R. and Nelson, C.: Geologically-consistent Multiphysics Imaging of the Darajat Geothermal Steam Field, *First Break*, **36**(6), (2018a), 77-83.

Soyer, W., Mackie, R.L. and Miorelli, F.: Optimizing the Estimation of Distortion Parameters in Magnetotelluric 3D Inversion, *80th EAGE Conference and Exhibition*, Copenhagen, Denmark (2018b).

Soyer, W., Mackie, R.L., and Miorelli, F.: Comparative Analysis and Joint Inversion of MT and ZTEM Data, *AEM, 7th International Workshop on Airborne Electromagnetics*, Kolding, Denmark (2018c).

Soyer, W., Miorelli, F. and Mackie, R.L.: Considering True Layout Geometry in Magnetotelluric Modeling *Extended Abstract*, 24th EM Induction Workshop, Helsingør, Denmark (2018d).

Soyer, W., Miorelli, F. and Mackie, R.L.: On the Effects of Finite Dipoles in 3-D Magnetotelluric Modeling, *81st EAGE Conference and Exhibition*, London, UK (2019).

Tietze, K., Ritter, O.: 3D Magnetotelluric Inversion in Practice - The Electrical Conductivity Structure of the San Andreas Fault in Central California, *Geophysical Journal International*, 195(1), (2013), 130-147.

Ussher, G., Harvey, C., Johnstone, R., and Anderson, E.: Understanding the Resistivities Observed in Geothermal Systems, *Proceedings, World Geothermal Congress*, Kyushu-Tohoku, Japan (2000).

Wannamaker, P.E., Stodt, J.A., and Rijo, L.: Two-dimensional Topographic Responses in Magnetotelluric Responses in Magnetotellurics Modeled Using Finite Elements, *Geophysics*, **51**(11), (1986), 2131-2144.

Watts, M.D., Mackie, R.L., Scholl, C. and Hallinan S.: Limitations of MT Static Shift Corrections Using Time-Domain EM Data, *Extended Abstracts*, SEG Annual Meeting, Houston, TX (2013).